The $O^{(n)}$ model on the triangular lattice

1998 J. Phys. A: Math. Gen. 31 2941

(http://iopscience.iop.org/0305-4470/31/13/005)

J. Phys. A: Math. Gen. **31** (1998) 2941–2966. Printed in the UK PII: S0305-4470(98)85293-1

The O(n) model on the triangular lattice

Yolanda M M Knops†§, Bernard Nienhuis‡ and Henk W J Blöte†

† Laboratorium voor Technische Natuurkunde, PO Box 5046, 2600 GA Delft, the Netherlands
‡ Instituut voor Theoretische Fysica, Universiteit van Amsterdam, Valckenierstraat 65, 1018 XE Amsterdam, the Netherlands

Received 23 June 1997

Abstract. To find critical points of O(n) models on the triangular lattice we apply two methods. First we investigate the Yang–Baxter equations on the triangular lattice. We find only solvable points directly related to those for the square lattice. Second we construct intersections with the Potts model. This yields eight branches of critical points, parametrized by n. We establish the equivalence of these branches with the known critical points of the O(n) model on the square lattice. Transfer-matrix calculations are performed to obtain the conformal anomaly and the thermal exponent of these branches. These results include a numerical analysis of a $q = 3$ Potts tricritical point. We find analytic relations between Potts and O(n) models, as well as among O(n) models with different values of n, and among Potts models with different values of q.

1. Introduction

The critical behaviour of the O(n) model, a model for n-component spins, has been studied on the honeycomb lattice [1] as well as on the square lattice [2, 3]. Using a method developed by one of us [1, 2], critical points of these models could be determined. For the honeycomb lattice two branches of critical points, parametrized by n, were found, describing the O(n) critical and low-temperature behaviour. For the square lattice five branches were found [2]. Two of them are generalizations of those of the branches of the honeycomb lattice and thus represent the critical and low-temperature behaviour. From a numerical analysis [3] it appeared that the other branches describe multicritical behaviour, a superposition of a low-temperature O(n) and a critical Ising model, and a point in the universality class of the low-temperature O($n + 1$) behaviour.

The partition sum of the O(n) model can be represented as the partition sum of a model of loops or polygons on the lattice [4]. This loop model is a continuous n generalization of the separable non-intersecting string model [5]. The critical point is caused by a balance between the energy and entropy of these loops, already possible on the honeycomb lattice. The multicritical behaviour on the square lattice is the result of an attractive interaction between polygons that meet at a vertex. Since the triangular lattice admits the possibility of three loops meeting in a single vertex, higher-order critical behaviour might be expected in this lattice. Therefore we have carried out two methods to obtain critical points. First we have studied Yang–Baxter (YB) equations on the triangular lattice for a fully packed loop model. These yielded non-trivial solutions which, however, could be identified with solutions already known for the square lattice. Second we have carried out a similar analysis for the O(n) model on the triangular lattice as was done for the square lattice in [2]. Using

§ Present address: TNO/TPD, PO Box 595, 5600 AN Eindhoven, the Netherlands.

0305-4470/98/132941+26$19.50

the method described therein we have found eight branches of critical points on the triangular lattice.

This method is based on the existence of renormalization mappings onto the Coulomb gas. Such mappings have been described for Potts models as well as for O(n) models [6]. This mapping of the Potts model at its critical temperature T_c leads to a Coulomb gas with even integer charges. Thermal deviations from T_c are associated with the appearance of positive unit charges. Negative unit charges correspond to non-Potts critical behaviour, because these negative charges cannot be translated into Potts-like variables. An O(n) model being mapped onto the Coulomb gas admits in general all integer charges. However, at the intersection of an O(n) model with a Potts model the negative unit charges disappear. Thus, at the intersection the O(n) model is critical, although the Potts model itself need not be critical. If the negative unit charges lead to a relevant scaling dimension, the O(n) model is critical in the sense that the free energy is singular as a function of the O(n) parameters. When this scaling dimension is irrelevant the O(n) model is still critical, but only in the sense that the correlations decay algebraically with distance.

In section 2 we describe the YB equations on the triangular lattice. In section 3 we obtain a number of intersections between a Potts model and an O(n) model using intermediate mappings onto a spin-$\frac{1}{2}$ and a spin-1 vertex model. This results in eight branches of O(n) critical points. In section 4 we investigate the relation of these branches with the critical branches on the square lattice. Two branches are also related to a Potts model on the triangular lattice. This is shown in section 5. A numerical analysis of the branches was carried out by means of transfer-matrix calculations. The specific problems for transfer-matrix calculations for the triangular O(n) model are treated in section 6. Section 7 contains the results of our calculations and section 8 gives the conclusions.

2. YB equations for the triangular lattice

We have checked for the possible presence of solvable models by solving the YB equations for the triangular lattice. These cover a larger parameter space than the corresponding equations for the square lattice, and could thus possibly yield new universality classes. To analyse the YB equations we have chosen a loop representation of the O(n) model (see section 3). We have restricted ourselves to a fully packed loop model such that all edges of the lattice are covered by a loop. The allowed loop configurations on a vertex of the triangular lattice appear in figure 6, with labels ρ_{10} and ρ_{11}. Taking into account rotated versions, there are five different vertices. Independent Boltzmann weights may be assigned to each of these. The weight of a loop is denoted n.

Although the loop representation has a non-local nature, it is still possible to formulate YB equations [7]. To this purpose, the lattice is divided in two parts: an internal part consisting of two adjacent lattice sites and the remaining external part. Separation of both parts leaves 10 'dangling bonds' for each part. Now replace the internal part by one of the configuration of three vertices shown in figure 1(a) (these also have precisely 10 dangling bonds). A graphical representation of the YB equations as shown in figure 1(a), expresses the condition that the interchange of both internal parts shown leaves the partition function invariant. Since the two vertices belonging to the original lattice interchange weights, and the process of replacement can be repeated indefinitely in one of the lattice directions, the YB equations guarantee that the vertex weights may be interchanged between two adjacent rows of vertices. Thus, the transfer matrices associated with both rows of spins commute. As a consequence of the existence of a family of commuting transfer matrices parametrized by a continuous parameter, exact solutions may be found [8].

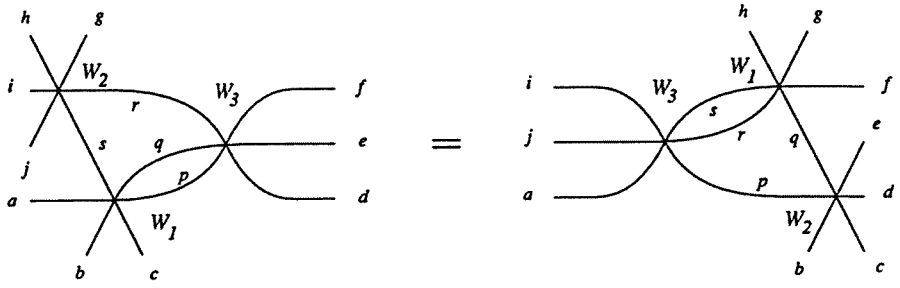

(*a*)

(*b*)

Figure 1. (*a*) YB equations for the triangular lattice. A summation of the Boltzmann weight over the internal indices on the left-hand side is required to produce the same result as the same for the right-hand side. This equality must hold for all possible choices of the external indices. (*b*) Example of a specific YB equation.

For a given a configuration of external vertices $\{v_e\}$ and internal vertices $\{v_i\}$, the Boltzmann weight consists of three factors. These are $u_e(\{v_e\})$ depending only on the exterior, $u_i(\{v_i\})$ depending only on the interior, and n^l where l is the number of loops that is closed when the two parts are connected. This number depends only on the way in which the dangling bonds of the internal part are interconnected by internal loop parts, and the same for the external dangling bonds. In other words, the number of loops closed by merging both lattice parts depends only on the internal connectivity $c_i(\{v_i\})$ and the external connectivity $c_e(\{v_e\})$. It is thus denoted $l(c_i, c_e)$. We note that the partition function of the loop model

$$Z = \sum_{\{v_e\}} u_e(\{v_e\}) \sum_{\{v_i\}} u_i(\{v_i\}) n^{l(c_i,c_e)} \tag{1}$$

can be rewritten

$$Z = \sum_{c_e} \sum_{c_i} \sum_{\{v_i\}|c_i} u_i(\{v_i\}) n^{l(c_i,c_e)} \sum_{\{v_e\}|c_e} u_e(\{v_e\})$$

or

$$Z = \sum_{c_i} U_i(c_i) P_e(c_i) \tag{2}$$

where $U_i(c_i) = \sum_{\{v_i\}|c_i} u_i(\{v_i\})$ and $P_e(c_i) = \sum_{c_e} \sum_{\{v_e\}|c_e} u_e(\{v_e\}) n^{l(c_i,c_e)}$. Now replace the internal part in line with figure 1(*a*) and denote the new internal weights by primed quantities u_i' and U_i'. Invariance of the partition sum implies that

$$\sum_{c_i} U_i(c_i) P_e(c_i) = \sum_{c_i} U_i'(c_i) P_e(c_i) \tag{3}$$

for which it is sufficient to require

$$U_i(c_i) = U_i'(c_i) \tag{4}$$

for all possible 10-point connectivities; this yields 42 equations. A specific equation is represented in figure 1(b). Another way to write the partition function is

$$Z = \sum_{c_e} W_i(c_e) U_e(c_e) \tag{5}$$

where

$$W_i(c_e) = \sum_{c_i} U_i(c_i) n^{l(c_i,c_e)} \tag{6}$$

and $U_e(c_e) = \sum_{\{v_e\}|c_e} u_e(\{v_e\})$. This yields a different way to formulate the invariance of the partition function, namely by requiring

$$W_i(c_e) = W_i'(c_e). \tag{7}$$

Note that equations (7) follow from equations (4) after multiplication by the matrix $n^{l(c_i,c_e)}$. Thus, at first sight it seems possible that equations (7) may allow more solutions than equations (4). However, we have checked that the matrix $n^{l(c_i,c_e)}$ is non-singular for general values of n; this shows that it is sufficient to solve the YB equations as expressed by equations (4).

We have set up the YB equations on the triangular lattice as a condition for the commutation of transfer matrices. When the vertices in the normal YB equations for the square lattice are interpreted not as Boltzmann weights but as collision amplitudes, the same equations can be viewed as a condition on the two-particle collision process necessary for the factorization of multiple-particle collisions into two-particle processes. In the same way, the YB equations for the triangular lattice can be viewed as a condition for factorization into three-particle collisions. Unfortunately all solutions to the triangular YB equations that we found, factorize into solutions of the square-lattice YB equation. Of course, this does not exclude the possibility that solutions without such a factorization exist in larger or different classes of models.

3. Derivation of the critical branches

As explained in the introduction, critical points of the O(n) model on the triangular lattice can be derived as the intersection of this model with a Potts model. The derivation of this intersection is quite similar to that for the case of Potts and O(n) models on the square lattice. For this reason we refrain from giving a detailed explanation of the mappings involved; for more details we refer to [2]. We consider the isotropic case and take into account the bulk properties only.

We start with a Potts model on the honeycomb lattice. At every site of the lattice is a q-state spin σ_i. Defining the interactions of this model by means of local Boltzmann weights, the weight W of an elementary hexagon is expressed in nearest-neighbour bond weights f_2 and face weights f_6:

$$W(\sigma_i, \sigma_j, \sigma_k, \sigma_l, \sigma_m, \sigma_n) = f_2(\sigma_i, \sigma_j) f_2(\sigma_j, \sigma_k) \cdots f_2(\sigma_n, \sigma_i) f_6(\sigma_i, \sigma_j, \sigma_k, \sigma_l, \sigma_m, \sigma_n) \tag{8}$$

where $i, j, \ldots, n$ label the spins clockwise, and

$$f_2(a, b) = [1 + x\delta_{ab}]^{1/2} \tag{9}$$

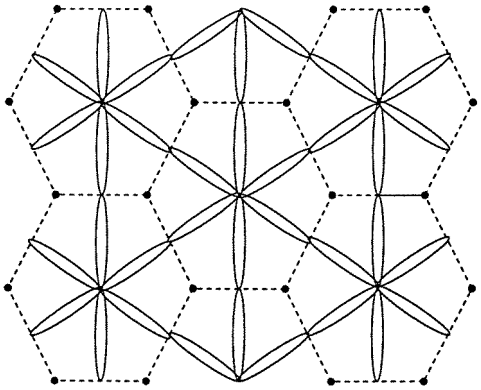

Figure 2. Surrounding lattice with the type-2 and type-6 vertices containing two and six leaves respectively.

and

$$f_6(a,b,c,d,e,f) = u + w(\delta_{ac} + \delta_{bd} + \delta_{ce} + \delta_{df} + \delta_{ea} + \delta_{fb}) + z(\delta_{ad} + \delta_{be} + \delta_{cf}) + r(\delta_{ac}\delta_{ce} + \delta_{bd}\delta_{df}) + s(\delta_{ac}\delta_{df} + \delta_{bd}\delta_{ea} + \delta_{ce}\delta_{fb}). \tag{10}$$

The weights x, w, r, s and z correspond to different types of bonds. The partition function is

$$Z = \sum_{\sigma_i} \prod_{\text{faces}} W(\sigma_i, \sigma_j, \sigma_k, \sigma_l, \sigma_m, \sigma_n). \tag{11}$$

It can be rewritten by expanding the product. Each term is represented by a graph displaying the δ_{ij} as bonds between pairs of spins i and j. By summing over the Potts spins we obtain

$$Z = \sum_{\mathcal{G}} q^{N_c} x^{N_x} w^{N_w} z^{N_z} r^{N_r} s^{N_s} u^{N_u} \tag{12}$$

where N_c is the number of components, and N_x, N_w, N_r, N_s, and N_z are the numbers of bonds of the type specified by the subscript according to the respective coefficients in f_2 and f_6. The number of empty faces is given by $N_u = N/2 - N_w - N_z - N_r - N_s$ where N is the total number of sites. The sum is over all graphs $\mathcal{G}$.

Following Baxter *et al* [9] this graph model can also be formulated as a loop model on the surrounding lattice. This lattice is shown in figure 2. It has two types of vertices, one with two leaves, and weight f_2, and one with six leaves, and weight f_6. Each graph $\mathcal{G}$ of equation (12) corresponds to a loop configuration $\mathcal{L}$ on the surrounding lattice as is shown in figure 3. The loops are uniquely defined by demanding that they do not intersect each other, that they do not cross the bonds of $\mathcal{G}$ and do cross the absent bonds. The number of loops can be expressed in properties of $\mathcal{G}$ by $N_l = N_c + N_i$, where N_l is the number of loops of $\mathcal{L}$ and N_i the number of inner circuits of $\mathcal{L}$, i.e. the number of loops of graph $\mathcal{G}$. Using Euler's relation $N_c = N - N_x - N_w - N_z - 2N_r - 2N_s + N_i$ the partition function becomes

$$Z = q^{N/2} \sum_{\mathcal{L}} \sqrt{q}^{N_l} \left(\frac{x}{\sqrt{q}}\right)^{N_x} \left(\frac{w}{\sqrt{q}}\right)^{N_w} \left(\frac{z}{\sqrt{q}}\right)^{N_z} \left(\frac{r}{q}\right)^{N_r} \left(\frac{s}{q}\right)^{N^s} u^{N_u}. \tag{13}$$

The sum is over all possible loop configurations covering the surrounding lattice.

This loop model is mapped onto a spin-$\frac{1}{2}$ vertex model by orienting the loops with arrows. Thus, each type-2 vertex and type-6 vertex has an ice-type configuration of

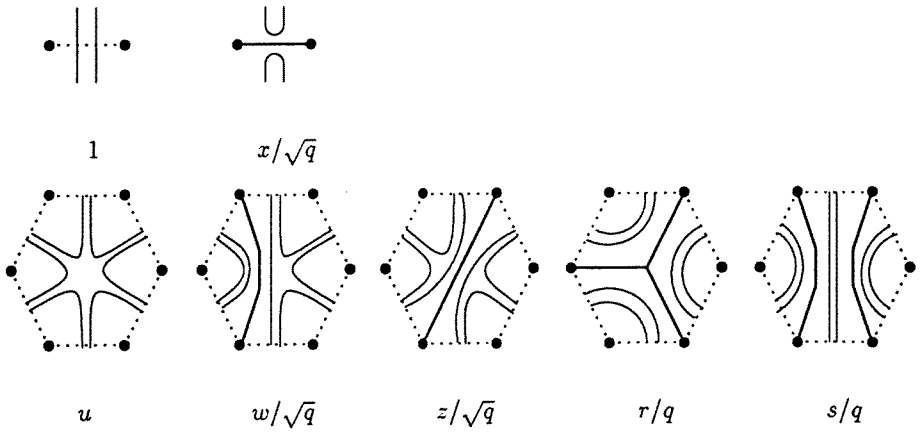

Figure 3. Relation between the graphs $\mathcal{G}$ and loops $\mathcal{L}$. The heavy lines between the sites represent the bonds in the graph representation. The other lines represent the corresponding loop segments in the loop representation.

arrows, the number of arrows pointing in is equal to the number of arrows pointing out. Following the loops in the direction of the arrows each turn of angle α is assigned a weight $\exp(\mathrm{i}\alpha\phi/2\pi)$. Summation over all possible orientations given a loop configuration contributes the prefactor $\sqrt{q}^{N_l}$ if ϕ is defined by

$$\sqrt{q} = \mathrm{e}^{\mathrm{i}\phi} + \mathrm{e}^{-\mathrm{i}\phi} = 2\cos(\phi). \tag{14}$$

The two terms account for the anticlockwise and clockwise orientation respectively.

The original partition function is recovered by first summing over all possible orientations of a given loop configuration and then summing over all loop configurations. When, however, the summation over the loop configurations is performed first given the orientation of each edge, one obtains a spin-$\frac{1}{2}$ vertex model. An example of how to calculate a spin-$\frac{1}{2}$ vertex weight is given in figure 4.

The spin-$\frac{1}{2}$ vertex model on the surrounding lattice can be mapped onto a spin-1 vertex model on the triangular lattice by combining the two spin-$\frac{1}{2}$ variables s_{i1} and s_{i2} on a leaf to a spin-1 variable S_i on a single edge. S_i is defined as $s_{i1}+s_{i2}$ and can take the values -1, 0 and 1. When $S_i = 0$, there is an internal degree of freedom, i.e. the sign of s_{i1}. The weights of the type-2 vertices can only be transferred to the type-6 vertices if this internal degree of freedom can be factorized. This factorization is realized for $x = -1$. The resulting spin-1

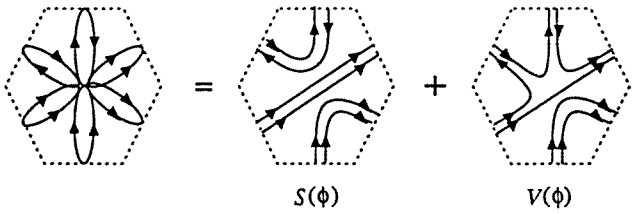

Figure 4. An example of how to calculate a spin-$\frac{1}{2}$ vertex weight on a type-6 vertex. This vertex has a weight $S(\phi) + V(\phi)$ where $S(\phi) = s\exp(-2\mathrm{i}\phi/3)/4\cos^2(\phi)$ and $V(\phi) = v\exp(\mathrm{i}\phi/3)/2\cos(\phi)$.

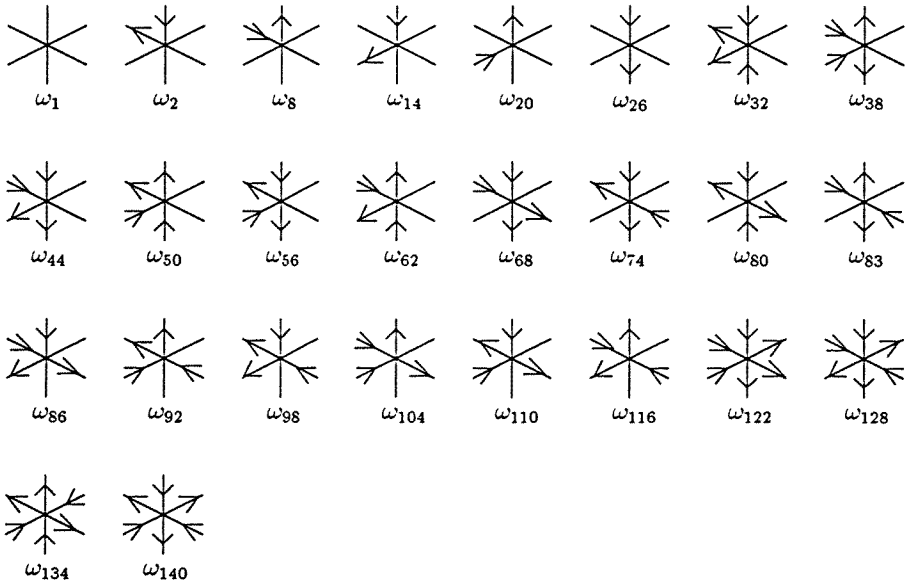

Figure 5. Spin-1 vertices on the triangular lattice with their Boltzmann weights. Vertices which are not shown are rotated versions of those shown, and have the same Boltzmann weight.

vertices are given in figure 5 and their weights are

$$
\begin{aligned}
w_1 &= 3s + 2r + 2w(12\cos(\phi)^2 - 9) + u(2\cos(4\phi) - 2\cos(\phi) + 1) + 12z(\cos(\phi)^2 - 1)\\
w_2 &= w_8^* = (4w + 2z)\mathrm{e}^{\mathrm{i}\frac{4}{3}\phi} + u\mathrm{e}^{\mathrm{i}\frac{10}{3}\phi} + (s + r - w - 2z)\mathrm{e}^{-\mathrm{i}\frac{2}{3}\phi} + w\mathrm{e}^{-\mathrm{i}\frac{8}{3}\phi}\\
w_{14} &= w_{20}^* = -u\mathrm{e}^{\mathrm{i}\frac{5}{3}\phi} - (2w + z)\mathrm{e}^{-\mathrm{i}\frac{1}{3}\phi} + z\mathrm{e}^{-\mathrm{i}\frac{7}{3}\phi}\\
w_{26} &= s + u + 2w\cos(2\phi)\\
w_{32} &= w_{38} = r - z + 2w\cos(2\phi)\\
w_{44} &= w_{50}^* = w\mathrm{e}^{\mathrm{i}\frac{4}{3}\phi} + s\mathrm{e}^{-\mathrm{i}\frac{2}{3}\phi}\\
w_{56} &= w_{62}^* = (w + u)\mathrm{e}^{\mathrm{i}\frac{8}{3}\phi} + (u + s + z + 3w)\mathrm{e}^{\mathrm{i}\frac{2}{3}\phi} + (w + r)\mathrm{e}^{-\mathrm{i}\frac{4}{3}\phi}\\
w_{68} &= -z\\
w_{74} &= s - 2z + 2w\cos(2\phi)\\
w_{80} &= w_{83}^* = (z + u)\mathrm{e}^{\mathrm{i}\frac{8}{3}\phi} + (u + 2z + 2w)\mathrm{e}^{\mathrm{i}\frac{2}{3}\phi} + s\mathrm{e}^{-\mathrm{i}\frac{4}{3}\phi}\\
w_{86} &= w_{98} = w_{92}^* = w_{104}^* = z\mathrm{e}^{\mathrm{i}\frac{5}{3}\phi} - w\mathrm{e}^{-\mathrm{i}\frac{1}{3}\phi}\\
w_{110} &= w_{116} = -2(z + w + u)\cos(\phi)\\
w_{122} &= s\\
w_{128} &= w_{134}^* = (r + w)\mathrm{e}^{\mathrm{i}\frac{2}{3}\phi} + (w + s)\mathrm{e}^{-\mathrm{i}\frac{4}{3}\phi}\\
w_{140} &= (12w + 4u)\cos(\phi)^2 + 2r\cos(2\phi) + 3s.
\end{aligned}
\tag{15}
$$

The others of the 141 weights w_k satisfy $w_k = w_{k-1}$, and correspond to rotated versions of the preceding vertex. All the weights were multiplied by the common factor of $4\cos(\phi)^2$.

For some choices of the weights this spin-1 vertex model can be transformed into special cases of an O(n) model, called 'branches'. This O(n) model consists of n-component unit

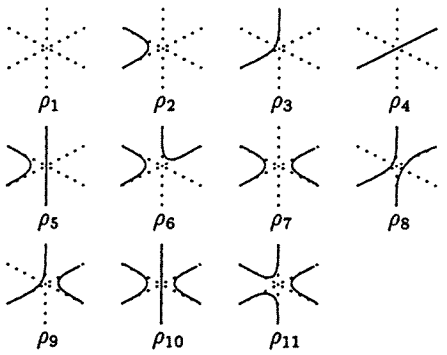

Figure 6. Loop configurations of the O(n) model on the vertices of the triangular lattice with their Boltzmann weights $\rho_1, \ldots, \rho_{11}$.

vectors, $\boldsymbol{s}$, living on the sites of a honeycomb lattice. The multispin interactions are defined by the Boltzmann weight, which is written as a product over the faces of the lattice:

$$\begin{aligned} W = \prod_{\text{faces}} [&\rho_1 + \rho_2(\boldsymbol{s}_i \cdot \boldsymbol{s}_j) + \rho_3(\boldsymbol{s}_i \cdot \boldsymbol{s}_k) + \rho_4(\boldsymbol{s}_i \cdot \boldsymbol{s}_l) + \rho_5(\boldsymbol{s}_i \cdot \boldsymbol{s}_l)(\boldsymbol{s}_j \cdot \boldsymbol{s}_k) \\ &+\rho_6(\boldsymbol{s}_i \cdot \boldsymbol{s}_j)(\boldsymbol{s}_k \cdot \boldsymbol{s}_l) + \rho_7(\boldsymbol{s}_i \cdot \boldsymbol{s}_j)(\boldsymbol{s}_l \cdot \boldsymbol{s}_m) + \rho_8(\boldsymbol{s}_i \cdot \boldsymbol{s}_k)(\boldsymbol{s}_l \cdot \boldsymbol{s}_n) \\ &+\rho_9(\boldsymbol{s}_i \cdot \boldsymbol{s}_k)(\boldsymbol{s}_l \cdot \boldsymbol{s}_m) + \rho_{10}(\boldsymbol{s}_i \cdot \boldsymbol{s}_l)(\boldsymbol{s}_j \cdot \boldsymbol{s}_k)(\boldsymbol{s}_n \cdot \boldsymbol{s}_m) \\ &+\rho_{11}(\boldsymbol{s}_i \cdot \boldsymbol{s}_j)(\boldsymbol{s}_k \cdot \boldsymbol{s}_l)(\boldsymbol{s}_m \cdot \boldsymbol{s}_n) + \text{other terms}]. \end{aligned} \tag{16}$$

The vectors are labelled with indices $i, j, \ldots, n$ in a clockwise fashion around each face. The other terms are obtained by cyclically permuting and inverting the indices i, j, k, l, m and n. A high-temperature expansion maps this model onto a dilute loop model on the triangular lattice [4]. Each term of the expansion represents a graph, consisting of a configuration of non-intersecting loops. Each loop has a weight n. The partition function of this O(n) loop model is

$$Z = \sum_{\mathcal{L}} n^{N_l} \rho_1^{N_1} \rho_2^{N_2} \cdots \rho_{11}^{N_{11}} \tag{17}$$

where $\rho_1, \ldots, \rho_{11}$ are the local weights of the loop configuration on a vertex as defined in figure 6. The sum is over all (dilute) loop configurations. The loop version of the O(n) model can be mapped onto a spin-1 vertex model by orienting the loops. In analogy with the Potts model a turn of angle α has a weight $\exp(\mathrm{i}\alpha\psi/2\pi)$. The loop weight n is then equal to $n = 2\cos\psi$.

Thus we have defined two spin-1 141-vertex models, one with parameters u, v, w, r, s and ϕ based on the Potts model, and one with parameters $\rho_1, \ldots, \rho_{11}$ and ψ based on the O(n) model. According to the argument described in the introduction, the intersection points of these two spin-1 vertex models are good candidates for critical points of the O(n) model. Equating the two sets of weights and eliminating $\rho_1 \cdots \rho_{11}$, four independent relations remain, namely

$$(u + 3w + z)\cos(\tfrac{2}{3}\phi) + r\cos(\tfrac{4}{3}\phi) + (u + w)\cos(\tfrac{8}{3}\phi) = (r + 2w\cos(2\phi) - z)\cos(\tfrac{2}{3}\psi) \tag{18a}$$

$$\begin{aligned} (u + 2w + 2z)\cos(\tfrac{2}{3}\phi) + s\cos(\tfrac{4}{3}\phi) + (u + z)\cos(\tfrac{8}{3}\phi) \\ = -z\cos(\tfrac{1}{3}\psi) + (s + 2w\cos(2\phi) - 2z)\cos(\tfrac{2}{3}\psi) \end{aligned} \tag{18b}$$

$$[z\cos(\tfrac{5}{3}\phi) - w\cos(\tfrac{1}{3}\phi)]\cos(\tfrac{1}{2}\psi) = -(u + w + z)\cos(\phi)\cos(\tfrac{1}{6}\psi) \tag{18c}$$

$$[(2u+6w)\cos(\phi)^2 + r\cos(2\phi)]\cos(\tfrac{1}{3}\psi)$$
$$= [(r+w)\cos(\tfrac{2}{3}\phi) + (s+w)\cos(\tfrac{4}{3}\phi) - s\cos(\tfrac{2}{3}\psi)]\cos(\psi). \quad (18d)$$

These equations lead to eight branches parametrized by n. The first two solutions have $u = w = z = 0$ and $\psi = 2\phi$ or $\psi = 2\phi - 3\pi$. We refer to them as branches 0 and 1. The O(n) weights follow as

$$\begin{aligned}
&\rho_1 = 3s + 2r,\ 3s + 2r\\
&\rho_2 = s + r,\ -(s + r)\\
&\rho_3 = \rho_8 = \rho_9 = 0,\ 0\\
&\rho_4 = \rho_7 = \rho_{10} = s,\ s\\
&\rho_5 = s,\ -s\\
&\rho_6 = r,\ r\\
&\rho_{11} = r,\ -r\\
&n = 2\cos(2\phi),\ -2\cos(2\phi)
\end{aligned} \quad (19)$$

where we have first denoted the weight of branch 0 and then, separated by a comma, that of branch 1. These branches contain a free parameter, namely the ratio of s and r.

The critical branches 2 and 3 come from the solution $s = 0$, $r = -w = -z = 1$ and $\psi = 4\phi - 3\pi$. The resulting weights are

$$\begin{aligned}
&\rho_1 = 64\sin(\phi)^6 - 2\cos(4\phi)\\
&\rho_2 = 16\sin(\phi)^4 + 1\\
&\rho_3 = 8\sin(\phi)^3 + 2\sin(\phi)\\
&\rho_4 = 8\sin(\phi)^2\\
&\rho_5 = \rho_8 = \rho_{11} = 1\\
&\rho_6 = \rho_7 = 4\sin(\phi)^2\\
&\rho_9 = 2\sin(\phi)\\
&\rho_{10} = 0\\
&n = -2\cos(4\phi).
\end{aligned} \quad (20)$$

For each value of n, ϕ can take two values, $\alpha = \frac{1}{4}\arccos(-n/2)$ and $\pi/2 - \alpha$ ($0 < \alpha < \pi/4$), which results in two independent branches, 2 and 3 respectively.

Four more critical branches come from the solution

$$\begin{aligned}
u &= -4\sin\left(2\phi - \frac{\pi}{3}\right)[\cos(5\phi) + 2\cos(3\phi) + \cos(\phi)]\\
s &= 8\sqrt{3}\sin(\phi)^2\sin\left(\phi + \frac{\pi}{6}\right)\\
z &= -16\cos\left(2\phi + \frac{\pi}{6}\right)\cos\left(\phi + \frac{\pi}{3}\right)\cos(\phi)^2\\
w &= 2\cos(\phi)^2\sin\left(\phi + \frac{\pi}{6}\right)\left[8\sin(2\phi)\sin\left(\frac{4}{3}\phi + \frac{\pi}{6}\right) - 4\sqrt{3}\cos\left(\frac{2}{3}\phi\right)\right]\Big/\cos\left(\frac{4}{3}\phi\right)\\
r &= 4[\cos(2\phi) + 1]\left[\sin\left(3\phi - \frac{\pi}{3}\right) + 2\sin\left(\phi + \frac{\pi}{3}\right) + \sin(\phi)\right]\\
\psi &= \pi - 4\phi.
\end{aligned} \quad (21)$$

This leads to the following weights

$$\begin{aligned}
\rho_1 &= 4\sin(\phi)\cos\left(8\phi+\frac{2\pi}{3}\right)-4\sqrt{3}\cos(5\phi)+4\sin(3\phi)+5\sqrt{3}\cos(\phi)+3\sin(\phi)\\
\rho_2 &= 2\sin(2\phi)\left[-2\cos(5\phi)+2\sqrt{3}\sin\left(\phi+\frac{\pi}{3}\right)\right]\\
\rho_3 &= 4\sin(2\phi)\sin\left(4\phi+\frac{\pi}{3}\right)\\
\rho_4 &= 2\cos\left(\phi-\frac{\pi}{3}\right)\left[2\sin\left(4\phi-\frac{2\pi}{3}\right)+2\sin\left(2\phi+\frac{2\pi}{3}\right)+\sqrt{3}\right]\\
\rho_5 &= 4\sin(2\phi)\cos\left(\phi-\frac{\pi}{3}\right)\\
\rho_6 &= 8\sin(2\phi)^2\sin\left(\phi+\frac{\pi}{3}\right)\\
\rho_7 &= 2\sin\left(5\phi-\frac{2\pi}{3}\right)-2\sin(3\phi)-4\sin\left(\phi-\frac{2\pi}{3}\right)\\
\rho_8 &= 4\sin\left(2\phi+\frac{2\pi}{3}\right)\cos\left(\phi+\frac{\pi}{3}\right)\\
\rho_9 &= 4\sin(2\phi)\sin\left(2\phi+\frac{2\pi}{3}\right)\\
\rho_{10} &= 2\sqrt{3}\cos\left(\phi-\frac{\pi}{3}\right)\\
\rho_{11} &= 8\sin\left(\phi+\frac{\pi}{3}\right)\cos\left(\phi-\frac{\pi}{3}\right)^2\\
n &= -2\cos(4\phi).
\end{aligned} \tag{22}$$

For each n there are four values of ϕ corresponding to different weights, namely $\phi = \alpha, \frac{\pi}{2}-\alpha, \alpha+\frac{\pi}{2}$ and, $\pi-\alpha$ $(0<\alpha<\pi/4)$. These are denoted branch 4, 5, 6 and 7 respectively.

4. The relation with the O(n) model on other lattices

For the O(n) model on the square lattice, five critical branches have been described [2, 3]. It is to be expected that the critical behaviour of these branches will be related in terms of universality to the O(n) model on the triangular lattice. For the critical branches 2–7 there exists a simple relation with the O(n) model on the square lattice. The weights of these branches are such that the O(n) model can be mapped onto the Kagomé lattice. This mapping replaces each vertex of the triangular lattice by three vertices of the Kagomé lattice (see figure 7(a)). These three vertices form an internal triangle. The Boltzmann weights of the Kagomé vertices are determined by demanding that the sum of the combined Kagomé weights over the internal indices is equal to the triangular weight for each choice of the external indices. Thus (see also figure 7(a))

$$\begin{aligned}
&\forall i, j, k, l, m, n:\\
&W(i,j,k,l,m,n)=\sum_{abc} W_K(n,i,b,a)W_K(j,k,c,b)W_K(l,m,a,c)
\end{aligned} \tag{23}$$

where $W(i, j, k, l, m, n)$ are the Boltzmann weights ρ_1–ρ_{11} of equations (19), (20) and (22), and W_K are the Boltzmann weights of the vertices on the Kagomé lattice. An example of a graphical representation of equation (23) can be found in figure 7(b).

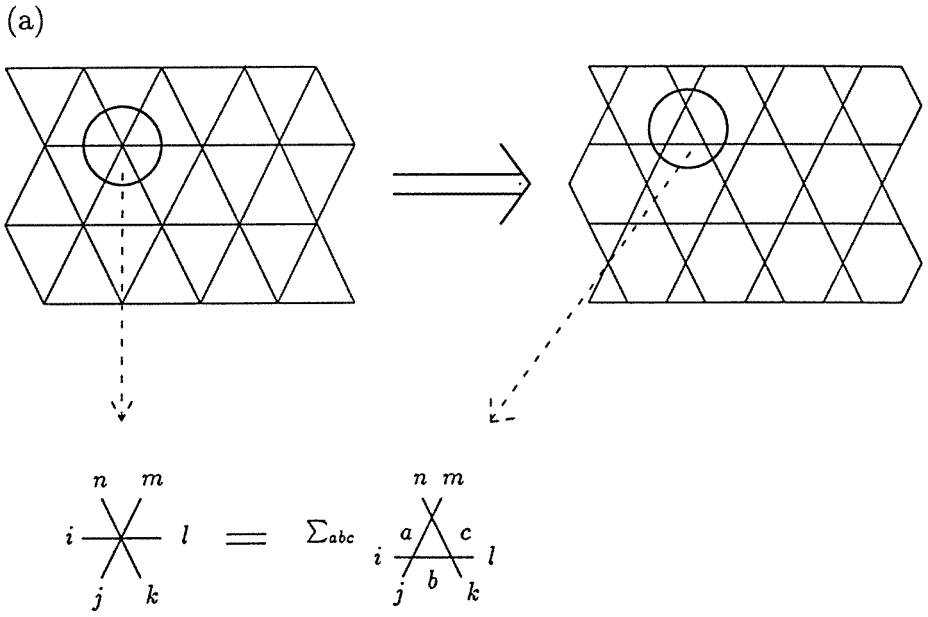

Figure 7. Relation between the triangular lattice and the Kagomé lattice. (*a*) Each vertex of the triangular lattice corresponds to three vertices of the Kagomé lattice as denoted in the circles. The weights of the Kagomé lattice obey equation (23), which is graphically represented. (*b*) An example of a graphical representation of equation (23).

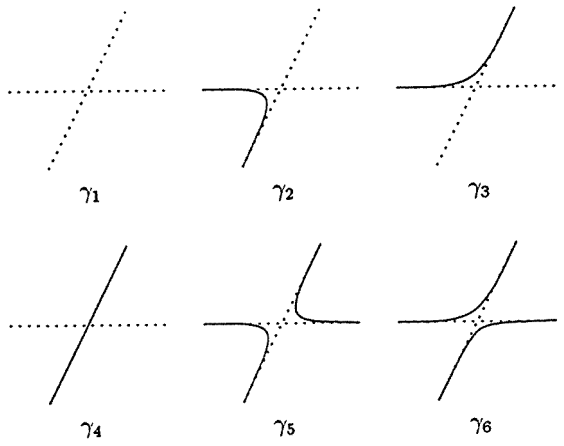

Figure 8. Loop configurations with Boltzmann weights on a Kagomé vertex.

The loop configurations on a Kagomé vertex are given in figure 8. For branches 2 and 3 the vertex weights γ and the loop weight n are

$$\begin{aligned}
&\gamma_1 = 4\sin(\phi)^2 \\
&\gamma_2 = \gamma_4 = \gamma_6 = 1 \\
&\gamma_3 = 2\sin(\phi) \\
&\gamma_5 = 0 \\
&n = -2\cos(4\phi)
\end{aligned} \tag{24}$$

where $\phi = \alpha$ and $\phi = \pi/2 - \alpha$ $(0 < \alpha < \pi/4)$ respectively. For branches 4–7 the Kagomé weights are

$$\begin{aligned}
&\gamma_1 = 4\cos\left(2\phi - \frac{\pi}{3}\right)\sin\left(\phi + \frac{\pi}{3}\right)\cos\left(\phi - \frac{\pi}{3}\right) - \sin(2\phi) \\
&\gamma_2 = \sin(2\phi) \\
&\gamma_3 = -2\sin(2\phi)\sin\left(\phi + \frac{\pi}{3}\right) \\
&\gamma_4 = \sin\left(2\phi + \frac{2\pi}{3}\right) \\
&\gamma_5 = \tfrac{1}{2}\sqrt{3} \\
&\gamma_6 = \sin(2\phi) + \tfrac{1}{2}\sqrt{3} \\
&n = -2\cos(4\phi)
\end{aligned} \tag{25}$$

where $\phi = \alpha, \pi/2 - \alpha, \alpha + \pi/2, \pi - \alpha$ $(0 < \alpha < \pi/4)$ respectively.

These two sets of weights (equations (24) and (25)) coincide with the general solution for the critical behaviour of the O(n) model on the square lattice as given in equation (15) of [2] for a special choice of the spectral parameter ψ in that equation. For the first set $\psi = \phi/2$ and for the second set $\psi = \phi/2 + 2\pi/3$. For each n the weights of equation (15) of [2] have four essentially different values, representing different critical behaviour. In figure 9 we have indicated for each value of ϕ and ψ the corresponding branch on the square lattice [10]. The two sets of Kagomé weights are denoted by the broken and dotted lines.

The model of equation (15) in [2] is solvable; it is known as the Izergin–Korepin model [11] and satisfies the YB equations. From analytical work [12] and numerical work [3] it follows that the solution is critical. In [3] the conformal anomaly and some critical dimensions were obtained using transfer-matrix calculations. These were done for the isotropic case of the model of equation (15) of [2], for which the spectral parameter is equal to $\psi = \pi/4$. It appeared that branches 1 and 2 of the O(n) model on the square lattice represent the critical behaviour and the low-temperature behaviour. These branches also occur on the honeycomb lattice [1, 2, 13]. Branch 3 represents the multicritical behaviour of a model with Ising and O(n) degrees of freedom and branch 4 describes a superposition of a critical Ising model and a low-temperature O(n) model. Later the conformal anomaly was also determined analytically (see [14]).

Because the weights on the Kagomé lattice satisfy the YB equations, the horizontal lines of the lattice can be shifted downwards, resulting in three square lattice parts. Therefore we may find the same behaviour for branches 2–7 on the triangular lattice as for the model on the square lattice.

Before we discuss the relation of branches 0 and 1 with the O(n) model on the Kagomé lattice, we first discuss their equivalence with a fully packed loop model. Because of a

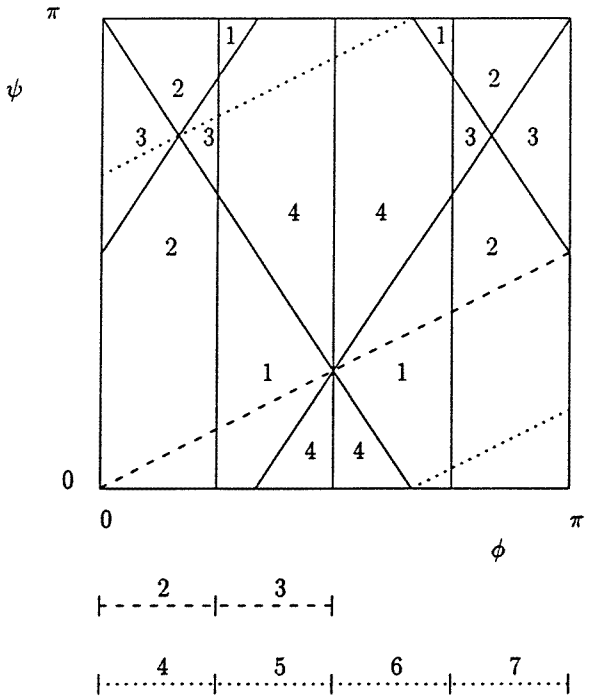

Figure 9. Comparison of O(n) models on different lattices. For each value of ϕ and ψ, used in equation (15) of [2] the corresponding branch on the square lattice is indicated by the numbers 1–4. The broken line represents the weight on the Kagomé lattice for which $\psi = \phi/2$, and the dotted line for which $\psi = \phi/2 + 2\pi/3$: the weights of equations (20) and (22) respectively. The corresponding branches on the triangular lattice are indicated on the bars below.

symmetry property of the partition function on the triangular lattice the fully packed model can be described by two equivalent sets of Boltzmann weights (see below). Branches 0 and 1 obey the same kind of symmetry. As a review of the relations between the fully packed loop model, branches 0 and 1 are given in table 1. The explanation is given below.

The fully packed O(n) loop model has only two non-zero vertex weights; $\rho_{10} = s$ and $\rho_{11} = r$. Because each contractible loop has an odd number of turns, we may include a minus sign in the weight of these turns, and compensate that with a minus sign in the weight of each contractible loop. We note that the number of non-contractible loops (those spanning the cylinder) is always even, at least for fixed boundary conditions at the ends of the cylinder. Thus, n may also be replaced by $-n$ for these loops. Thus the partition sum Z_f of the fully packed loop model satisfies

$$Z_f(s, r, n) = Z_f(s, -r, -n). \tag{26}$$

There is an inversion symmetry in the (r, n) plane with respect to (0,0).

Next we interpret Z_f as the partition sum of a two-coloured loop model; loops are either red or blue. The red loops have weight $n - 1$, and the blue loops have weight 1. Summing over all possible ways to colour the loops will thus reproduce the correct loop weight n. Because the blue loops have weight 1, their degrees of freedom are independent and can be summed out given a configuration of red loops. What remains is a dilute loop model with loop weight $n - 1$ and a partition function Z_0 satisfying

$$Z_0(s, r, n - 1) = Z_f(s, r, n). \tag{27}$$

Table 1. Equivalences between the two fully packed representations (above) and the two dilute representations of branches 0 and 1. The operator N changes the sign of the loop weight, as well as that of some vertex weights as described in the text. The operators ± 1 transform the dense O(n) loop models into dilute models with loop weights $n \mp 1$. From the left to the right, the columns represent branch 0 with parameters s, r and $n-1$; branch 1 with s, $-r$ and $n+1$; branch 0 with s, $-r$ and $-n-1$; and branch 1 with s, r and $-n+1$. Only the non-zero weights are shown.

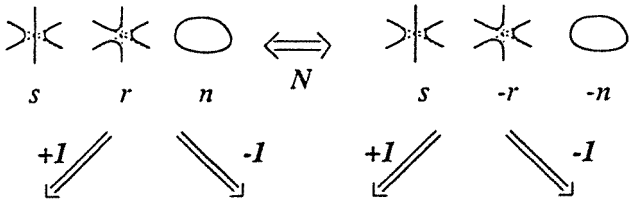

	3s+2r	3s-2r	3s-2r	3s+2r
	s+r	-s+r	s-r	-s-r
	s	s	s	s
	s	-s	s	-s
	r	-r	-r	r
	s	s	s	s
	s	s	s	s
	r	r	-r	-r
	n-1	n+1	-n-1	-n+1

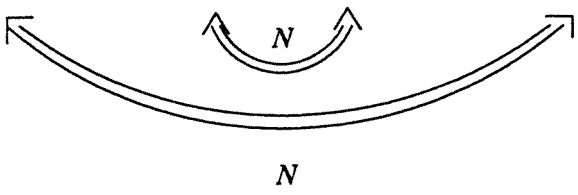

The vertex weights of branch 0 are obtained by a summation over the blue degrees of freedom. For example the weight of a type-2 vertex is $r+s$, because it can be covered by vertices of type 10 and 11 (with two blue loop parts and one red loop part).

Using equation (26), this mapping can equivalently be applied to the fully packed model with the weights s, $-r$ and $-n$. This yields an equivalent set of Boltzmann weights for branch 0, as shown in the third column of table 1. Thus for branch 0 we have

$$Z_0(s, r, n-1) = Z_0(s, -r, -n-1). \tag{28}$$

In this case the inversion symmetry in the (r, n) plane is with respect to the point $(0, -1)$.

Also, branch 1 can be derived from the fully packed model, and can thus be described by two sets of Boltzmann weights. The first set is obtained by starting from the fully packed model with weights s, r and n. This is equivalent to a two-colour loop model, where the red loops have weight $n+1$ and the blue loops have weight -1. In order to compensate the factor of -1 in the weight of a blue loop, we assign a factor of -1 to each blue turn. For the blue loops around the cylinder a seam of modified vertex weights is added to compensate the factor of -1. Summing out the blue degrees of freedom we obtain the O$(n+1)$ dilute loop model with the bulk weights of branch 1 (see equation (19)). Thus

$$\tilde{Z}_1(s, -r, n+1) = Z_f(s, r, n) \tag{29}$$

where $\tilde{Z}$ is the partition function of the cylinder with a seam. The bulk weights are given in the second column of table 1.

Starting from the fully packed model with weights s, $-r$ and $-n$, the second set of Boltzmann weights is obtained in the same way. These weights are given in column 4 of table 1 and in equation (19). Thus, for branch 1 the symmetry relation is

$$\tilde{Z}_1(s, -r, n+1) = \tilde{Z}_1(s, r, -n+1). \tag{30}$$

The inversion symmetry is with respect to $r = 0$ and $n = 1$.

Since branches 0 and 1 can be mapped onto the fully packed model, they must be equivalent. This equivalence is easily shown without using the fully packed model. It is possible to compensate the minus sign of the loop weight, because only sharp turns are allowed and each contractible loop has an odd number of turns. Loops spanning the cylinder obtain the right weight when a seam is added in the case of branch 1. The weights of column 4 are obtained from those of column 1 by changing the signs of the loop weight and of the weights of the vertices with an odd number of sharp turns. The same holds for the weights in columns 2 and 3 in table 1. Thus

$$Z_0(s, r, n) = \tilde{Z}_1(s, r, -n). \tag{31}$$

We show the relation of branches 0 and 1 with the O(n) model on the Kagomé lattice using the same kind of relation for the fully packed model. For two ratios s/r the triangular fully packed loop model can be mapped onto a fully packed loop model on the Kagomé lattice. Solving equation (23) with only non-zero weights ρ_{10}, ρ_{11}, γ_5, γ_6 and n it follows that the two solutions are given by $\rho_{10} = s = 2r\cos(2\phi/3)$, $\rho_{11} = r$, $n = 2\cos(2\phi)$, $\gamma_5 = r^{1/3}[2\cos(2\phi/3)]^{-2/3}$ and $\gamma_6 = [2r\cos(2\phi/3)]^{1/3}$ and by $\rho_{10} = s = 2r\cos(2\phi/3)$, $\rho_{11} = -r$, $n = -2\cos(2\phi)$, $\gamma_5 = -r^{1/3}[2\cos(2\phi/3)]^{-2/3}$ and $\gamma_6 = [2r\cos(2\phi/3)]^{1/3}$. In [15] it is shown that the O(n) model with only non-zero weights γ_5 and γ_6 satisfies the YB equations. Thus the Kagomé lattice can be transformed into three square lattices. The weights for the fully packed loop model on the Kagomé lattice can also be mapped, via a two-colour model, on a dilute loop model with loop weight $n-1$ for the first solution and with loop weight $-n-1$ for the second solution. Thus, two points of branch 0 on the square lattice are obtained as described in equation (12) of [2]. From the numerical work [3] it appears that this branch with loop weight n is equivalent to the low-temperature behaviour of the O$(n+1)$ model of branch 2.

From the existence of two exactly solvable points for the fully packed loop model it follows that branch 0 also has two sets of exactly solvable points. The first set is described by $s = 2r\cos(2\phi/3)$, $r = r$ and $n = 2\cos(2\phi) - 1$ and the second set is described by $s = 2r\cos(2\phi/3)$, $r = -r$ and $n = -2\cos(2\phi) - 1$. If the weights of the loops are given by n' we expect for the first set of weights a low-temperature $O(n' + 1)$ behaviour and for the second set a low-temperature $O(-n' - 1)$ behaviour.

Also, branch 1 with seam has two sets of points which can be mapped onto the Kagomé lattice, namely $\rho_{10} = s = 2r\cos(2\phi/3)$, $\rho_{11} = r$ and $n = 2\cos(2\phi) + 1$ and $\rho_{10} = s = 2r\cos(2\phi/3)$, $\rho_{11} = -r$ and $n = -2\cos(2\phi) + 1$. Thus, for these points we expect low-temperature $O(n' - 1)$ behaviour and low-temperature $O(-n' + 1)$ behaviour respectively.

5. Relation of branches 0 and 1 with Potts models

The fully packed loop model, defined in section 4, not only describes branches 0 and 1 of the O(n) model, but it also describes the self-dual line of a q'-state Potts model with $\sqrt{q'} = 2\cos(2\phi) + 1$. This Potts model can thus be transformed into the q-state Potts model ($\sqrt{q} = 2\cos(\phi)$), defined in section 3. This will be shown below.

The q'-state Potts model is defined on the triangular lattice. Triangular lattice Potts models with three-spin interactions in all triangles are described in [16]. Here, at every site there resides a Potts spin σ_i with nearest-neighbour couplings J and three-spin couplings K only in the left triangles. The partition function is given by

$$Z = \sum_{\sigma} \prod_{\triangleleft} [1 + a(\delta_{\sigma_i\sigma_j} + \delta_{\sigma_j\sigma_k} + \delta_{\sigma_k\sigma_i}) + b\delta_{\sigma_i\sigma_j\sigma_k}] \tag{32}$$

where $1 + a = \exp(J)$ and $1 + 3a + b = \exp(3J + K)$ and the product is over all triangles pointing to the left. Equation (32) can also be rewritten as the partition function of a loop model with loop weight $\sqrt{q'}$ and with vertex weights $1, a/\sqrt{q'}$ and b/q' (see figure 10). Duality indicates that the model is critical for $b/q' = 1$ [17]. This can easily be seen by comparing this model with a Potts model with three spin interactions only in the triangles pointing to the right. The model also coincides with the fully packed representation of branches 0 and 1 of the O(n) model on the triangular lattice, with $\sqrt{q'} = 2\cos(2\phi) + 1$ and $s/r = a/\sqrt{q}$.

The relation of branches 0 and 1 on the one hand with a Potts model with $\sqrt{q} = 2\cos(\phi)$, and on the other hand with a Potts model with $\sqrt{q'} = 2\cos(2\phi) + 1$, can be seen directly. The Potts model on the honeycomb lattice defined in equation (13) with $u = w = z = 0$ and $x = -1$ can be mapped onto the Potts model on the triangular lattice, defined in equation (32), at its self-dual line ($b = q'$). The mapping is as follows. We start with the loop representation of the Potts model on the honeycomb lattice (see equation (13)). Because $u = w = z = 0$ loops occur only in the form of double-loop segments (segments of these double loops are separated by the Potts bond variables). This makes it possible to

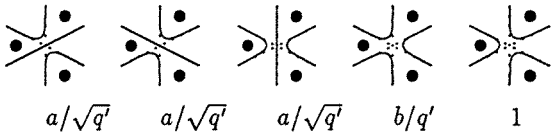

Figure 10. Loop configurations for the Potts model on the triangular lattice with their Boltzmann weights. The full circles represent the Potts spins of the triangular lattice.

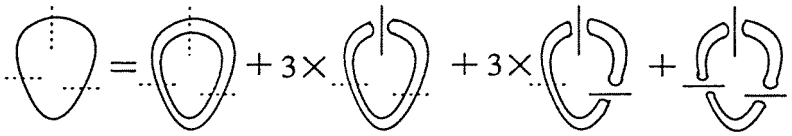

Figure 11. Correspondence between the loop weights of two Potts models. One single loop with weight $q-1$ represents the sum over all bond configurations on the edges crossed by a pair of loops with loop weight $\sqrt{q}$. The weight of a bond is $-1/\sqrt{q}$.

sum out the bonds on the edges given a configuration of the allowed vertices. If there are no bonds on the edges the configurations consist of $N_l/2$ double loops. These configurations are denoted $\mathcal{L}'$. The bonds can be summed out independently for each pair of loops, thus the partition sum is written as

$$Z = \sum_{\mathcal{L}'} \left(\frac{r}{q}\right)^{N_r} \left(\frac{s}{q}\right)^{N_s} \sqrt{q}^{N_l} \prod_{\text{double loops}} \left[\tilde{\sum_{\text{bonds}}} \left(\frac{x}{\sqrt{q}}\right)^{m} \sqrt{q}^{\Delta N_l}\right] \tag{33}$$

where $\tilde{\sum}_{\text{bonds}}$ is a sum over the bonds on all the edges that are crossed by a certain double loop, m is the number of placed bonds on the double loop and ΔN_l is the change in the number of loops by placing the bonds on the edges. The first present bond decreases the number of loops by 1, the following bonds increase the number of loops by 1 (see figure 11). Thus, if N_e is the number of edges that cross a double loop, the summation over the bonds leads to

$$1 + \sum_{m=1}^{N_e} \binom{N_e}{m} \left(\frac{x}{\sqrt{q}}\right)^{m} \sqrt{q}^{m-2}. \tag{34}$$

Using Newton's binomium and $x=-1$ this is equal to $1-1/q$. Because we have summed out the bonds on the edges only double loops remain. These can be replaced by single loops with a weight $q-1 = 2\cos(2\phi)+1$. The vertices of this loop model are precisely those of figure 10. Thus, from the loop representation of the q-state Potts model on the honeycomb lattice we have derived the loop representation of the q'-state Potts model on the triangular lattice at its self-dual line. The relation between both Potts models is $\sqrt{q'} = q-1$. These Potts models are of a different nature: the honeycomb model is a zero-temperature antiferromagnet (as far as nearest-neighbour pairs are concerned), while the triangular model is in the critical state separating the ordered and disordered phases.

The relation between the two Potts models can be seen even more directly if they are treated as Temperley–Lieb models [17]. The corresponding adjacency diagrams are drawn in figure 12. The largest eigenvalue of the adjacency matrix is the loop weight [18]. In this case they are $q-1$ and $\sqrt{q'}$ for the honeycomb and the triangular lattice respectively. The models are only equivalent if the loop weights equal, thus $\sqrt{q'} = q-1$.

6. The transfer-matrix calculations

To obtain the free energy per site and the correlation length of these eight branches we have performed transfer-matrix calculations. The construction of a transfer matrix for the loop model on the square lattice is described in some detail in [3]. It requires a coding of O(n) connectivities by means of the integers $1, 2, 3, \ldots$, which serve as transfer-matrix indices. This coding is directly applicable to the O(n) model on the triangular lattice; however, the sparse matrix method for the triangular lattice remains to be explained.

Figure 12. Adjacency diagrams of the q'-state Potts model on the triangular lattice and of the q-state Potts model on the honeycomb lattice.

The transfer matrix is defined in the following way. The loop model on the triangular lattice is wrapped onto a cylinder with circumference L. The transfer matrix $\mathbf{T}$ adds an extra row to the cylinder, thus the action of $\mathbf{T}$ is expressed by

$$\boldsymbol{Z}_L^{(M+1)} = \mathbf{T}_L \cdot \boldsymbol{Z}_L^{(M)} \tag{35}$$

where $\boldsymbol{Z}_L^{(M)}$ is a vector of restricted partition functions with a connectivity α of a cylinder with circumference L and length M.

By factorizing the transfer matrix into sparse matrices, which add only one vertex, the computer time and memory requirements are reduced enormously. For a triangular lattice we need three types of sparse matrices, $\mathbf{T}_L = \mathbf{T}_l \cdot (\mathbf{T}_m)^{(L-2)} \cdot \mathbf{T}_b$. Adding a new row, we start with a complete last row which has $2L$ dangling bonds (see figure 13(a)). $\mathbf{T}_b$ adds the first vertex of a new row, resulting in a cylinder with $2L+2$ dangling bonds (see figure 13(b)). $\mathbf{T}_m$ adds the following vertex and is also used for the following $L-3$ vertices (see figure 13(b)). Then $\mathbf{T}_l$ completes the new row and thus reduces the number of dangling bonds from $2L+2$ to $2L$ again. The matrices do not only add a new vertex, but also permute the vertices in such way that the same $\mathbf{T}_m$ can be used for $L-2$ vertices.

The programming of these sparse matrices is rather tedious for the triangular lattice because there are many possible ways to add a new vertex, in comparison with the square lattice. Fortunately for branches 0 and 1 all turns $2\pi/6$ have weight 0. This reduces the number of possibilities which makes the programming practicable.

For branches 2–7 the transfer matrix can be factorized in even more sparse matrices because these branches can be mapped onto the Kagomé lattice. For each triangular vertex which is added three Kagomé vertices are added. From figure 14 it can be seen that some of these sparse matrices will be equivalent provided that the right permutation of dangling bonds has been carried out. The transfer matrices for the triangular vertices factorize into (see figure 14)

$$\begin{aligned} \mathbf{T}_b &= \mathbf{T}_3 \cdot \mathbf{T}_2 \cdot \mathbf{T}_1 \\ \mathbf{T}_m &= \mathbf{T}_3 \cdot \mathbf{T}_4 \cdot \tilde{\mathbf{T}}_1 \\ \mathbf{T}_l &= \mathbf{T}_5 \cdot \mathbf{T}_4 \cdot \tilde{\mathbf{T}}_1 \end{aligned} \tag{36}$$

where $\mathbf{T}_2$ increases the number of dangling bonds by 2 and $\mathbf{T}_5$ reduces it by 2. The matrix $\mathbf{T}_1$ works in the space with $2L$ dangling bonds and $\tilde{\mathbf{T}}_1$ in the space with $2L+2$ dangling bonds. Thus the transfer matrix now factorizes into

$$\mathbf{T} = \mathbf{T}_5 \cdot \mathbf{T}_4 \cdot \tilde{\mathbf{T}}_1 \cdot (\mathbf{T}_3 \cdot \mathbf{T}_4 \cdot \tilde{\mathbf{T}}_1)^{(L-2)} \cdot \mathbf{T}_3 \cdot \mathbf{T}_2 \cdot \mathbf{T}_1. \tag{37}$$

The free energy per unit of area f_L and the correlation length ξ_L^{-1} of a cylinder with circumference L are determined by the largest two eigenvalues λ_0 and λ_1 of $\mathbf{T}$,

$$f_L = \zeta \tfrac{1}{L} \log \lambda_0 \tag{38}$$

$$\xi_L^{-1} = \zeta \log(\lambda_0/\lambda_1) \tag{39}$$

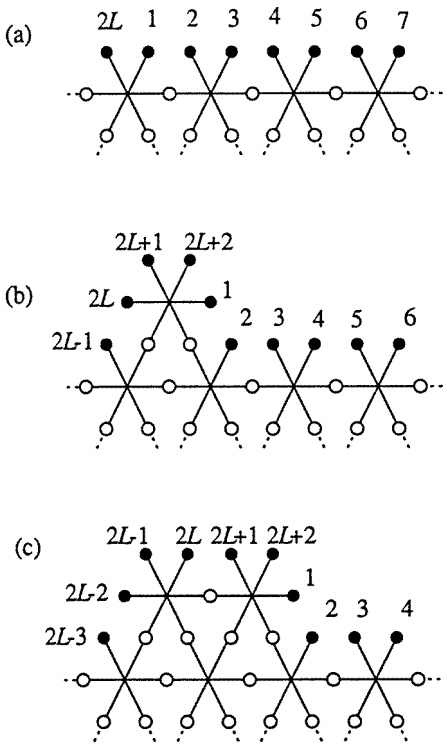

Figure 13. Topmost row of an O(n) model wrapped on a cylinder with width L. The circles denote the dangling bonds and coincide with the sites of the O(n) spins. The open circles are in the bulk of the lattice and the full circles are on the boundary. (a) Situation with a complete row. There are $2L$ dangling bonds. (b) Situation after addition of the first vertex by $\mathbf{T}_b$. The number of dangling bonds is increased by two. (c) Situation after addition of the second vertex by $\mathbf{T}_m$. The vertices are permuted such that $\mathbf{T}_m$ can also be used to add the following vertices. The number of dangling bonds remains the same. Adding the last vertex by $\mathbf{T}_l$ decreases the number of dangling bonds by two, and the situation of (a) is back.

except in special cases that will be discussed later. ζ is the geometrical factor, for the triangular lattice $\zeta = 2/\sqrt{3}$. These eigenvalues are calculated numerically using a direct iteration Hessenberg algorithm as described in [19].

From the theory of conformal invariance [20], relations follow between the free energy and the conformal anomaly c and between the correlation length and the anomalous dimension x (of the pertaining correlation function). Namely

$$f_L \simeq f_\infty + \frac{\pi c}{6L^2} \tag{40}$$

$$\xi_L^{-1} \simeq \frac{2\pi x}{L}. \tag{41}$$

Thus an analysis of the results for finite systems, using an iterated fit procedure as described in [3] yields the determination of c and x.

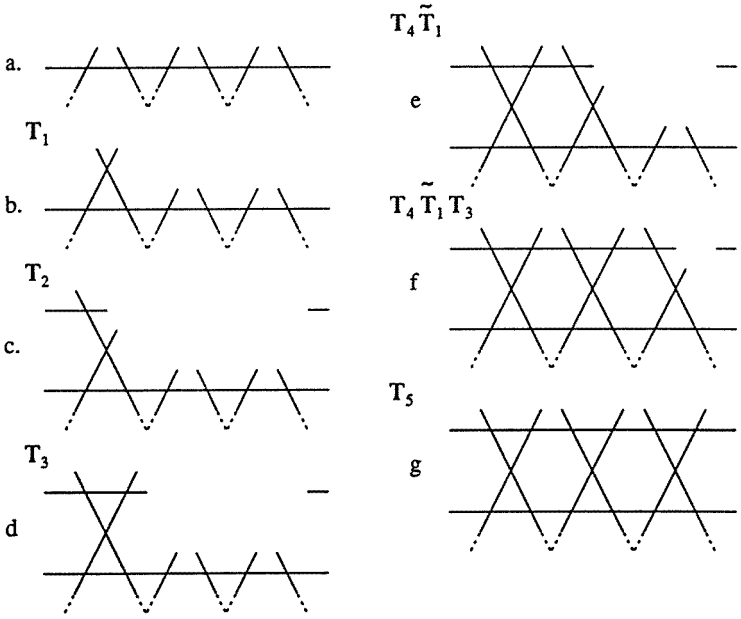

Figure 14. Topmost rows of the O(n) model on the Kagomé lattice wrapped on a cylinder with finite size three. Going from (a) to (g) we have represented the action of the transfer matrices $\mathbf{T}_1, \ldots, \mathbf{T}_5$ as indicated in the figure. Thus, the situation in (b) is obtained from the situation in figure 14(a) after multiplication by $\mathbf{T}_1$.

7. Results

We have determined the two leading eigenvalues for branches 0–7 of the O(n) model on the triangular lattice to determine the conformal anomaly and the thermal exponent. We will first discuss the results for branches 2–7 and then the results for branches 0 and 1.

7.1. Branches 2–7

Transfer-matrix eigenvalues for the triangular O(n) model were obtained by using the equivalent model on the Kagomé lattice (section 4). The results for the conformal anomaly and the thermal exponent for branches 2–5 can be found in tables 2 and 3. It follows from these results that we may identify the universality classes of these branches with those of branches 2, 1, 3 and 4 on the square lattice respectively [3]. This is also illustrated in figure 9. Thus, branch 3 describes the O(n) critical behaviour, branch 2 describes the O(n) low-temperature behaviour, branch 4 describes the multicritical behaviour of a model with O(n) and Ising degrees of freedom, and branch 5 the behaviour of a low-temperature O(n) model plus a critical Ising model. From figure 9 it can be seen that branch 4 has a special point for $n = 1$; at this point the analytic form of the conformal anomaly changes [14].

From figure 9 we can see that branches 6 and 7 should be identified with branches 1 and 4 and with branch 2 on the square lattice. However, this is not confirmed by the numerical results, the results for branches 6 and 7 do not converge. This may be related to the following. The weight γ_2, a vertex with a sharp turn, on the square lattice is determined up to a sign, because the number of these vertices is always even. However, for the Kagomé lattice the number of these vertices can also be odd. Thus if the weight γ_2 is negative the

Table 2. The conformal anomaly c for branches 2–5. We have used data for finite size 2 to 7. Estimated uncertainties in the last decimal places are given between parentheses.

n	Branch 2	Branch 3	Branch 4	Branch 5
2.0	1.000 0(1)	1.000 0(1)	1.500(1)	1.500(1)
1.5	0.587 57(1)	0.741 83(2)	1.275(5)	1.088(1)
1.0	0	0.500 000(1)	1.005(3)	0.500 00(1)
0.5	−0.820 0(1)	0.255 95(5)	0.560(1)	−0.320(1)
0.0	−2.000(1)	0	0	−1.500(1)
−0.5	−3.81(1)	−0.279 00(5)	−0.35(1)	−3.31(1)
−1.0		−0.600 00(1)	−0.600 00(1)	−6.52(3)
−1.5		−1.009 7(1)	−0.821(1)	
−2.0		−1.89(1)	0	

Table 3. The thermal exponent x_t for branches 2–5. We have used data for finite size 2–7. Estimated uncertainties in the last decimal places are given between parentheses.

n	Branch 2	Branch 3	Branch 4	Branch 5
2.0	2.0000(1)	2.000 0(1)		
1.5		1.251 89(1)	0.63(2)	1.000 0(1)
1.0		1.000 00(1)	0.47(1)	1.000 00(1)
0.5		0.817 8(1)	0.24(1)	1.000 0(1)
0.0		0.666 7(1)	0.15(1)	1.000 00(1)
−0.5		0.531 0(1)	0.216(1)	1.000 0(1)
−1.0		0.400 0(1)	0.400 00(1)	1.000 (1)
−1.5		0.260(1)	0.610 1(1)	
−2.0		0.03(3)		

partition function on the Kagomé lattice will be different as on the square lattice. For branches 6 and 7, γ_2 is negative; thus we might expect to find different behaviour as on the square lattice.

7.2. Branches 0 and 1

As explained in section 4, branches 0 and 1 have two different kinds of loop representations; a dilute loop representation and a fully packed loop representation. The fully packed model is not only equivalent to the branches 0 and 1, but also with a Potts model on the triangular lattice (equation (32)). The results for branches 0 and 1 have to be consistent with the known results for the Potts model in the region where it is physical (i.e. the Potts model has positive Boltzmann weights). We discuss the results for branch 0 in more detail. The results for branch 1 with a seam (see section 4) are similar.

We have determined the largest eigenvalue of the transfer matrix for the dilute representation as well as for the fully packed representation, for several values of n and θ. The ratio s/r (see equation (19)) is parametrized as $s/r = \tan(2\pi\theta)$. It appears that for both representations a crossing of eigenvalues occur, indicating a first-order transition between two regions of different behaviour (see figure 15). However, for one region the leading eigenvalues of the two representations are not the same. This result is rather paradoxical. The association the largest eigenvalue of $\mathbf{T}$ with the free energy would imply that the free energies of both representations are different. However, the mapping between the two loop models was constructed such that the partition sum remains invariant.

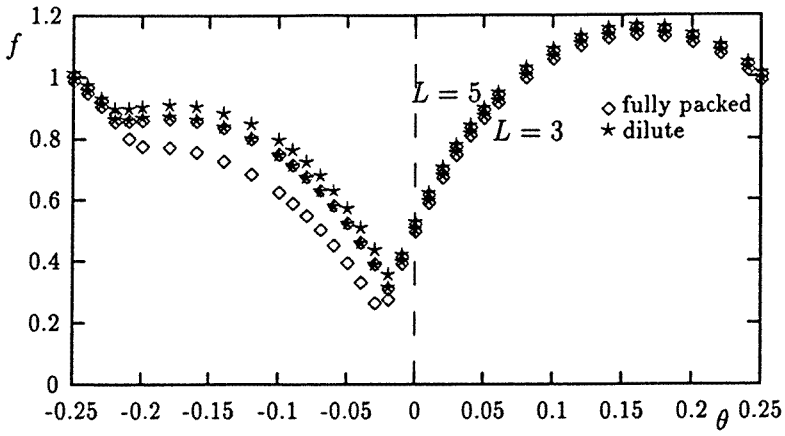

Figure 15. Free energy per site of branch 0 as a function of θ for $n = 0.5$ for the fully packed representation and for $n = -0.5$ for the dilute representation. Data are shown for $L = 3$ and $L = 5$. The discontinuity in the derivative of the free energy indicates the first-order transition.

The solution of this paradox is as follows. Since it has not yet been determined whether the leading eigenvalues of the transfer matrices do actually contribute to the partition function, it is possible that their contribution vanishes when closing the dangling bonds of the cylinder with appropriate begin and end vectors. The ith element of the end vector is, apart from a constant factor, equal to n^{N_i}, where N_i is the number of loops closed by the addition of the end row with some specified connectivity, prior to which the last row of the cylinder had connectivity i. We have calculated the inproduct of the eigenvectors of the dilute transfer matrix with the end vectors for $L = 2$ and $L = 3$. It appears that only those eigenvalues which also occur in the fully packed transfer matrix, contribute to the partition function.

Therefore we have based our calculation the conformal anomaly of the triangular O(n) model on the largest eigenvalue for the fully packed representation. The results are shown in figure 16. For each n there is a range of low-temperature O($n+1$) behaviour and a range of low-temperature O($-n-1$) behaviour.

Another curious phenomenon is that for $q = 1, 2, 3$ the transition between the O($n+1$) and O($-n-1$) behaviour takes place in the region where the Potts model is physical, i.e. negative Boltzmann weights are absent. This region is to the left of the dotted line and above the line $n = -1$ in figure 16. This would seem to indicate the existence of physical Potts models with non-unitary behaviour, e.g. c is negative for the relevant O($-n-1$) model. This would be a very strange situation.

However, after closing the fully packed transfer matrix for $q = 1, 2, 3$ with physical end vectors which include the weights of the loops that are closed, it appears that the contribution associated with the largest eigenvalue vanishes. Remarkably, this contribution does not vanish for general q.

The behaviour of the Potts model is thus determined by subdominant eigenvalues, leading to a non-negative c. On the boundary of the physical region ($a = -1$) the conformal anomaly changes to $c = 0$ for integral values of q, because all spins are frozen out.

For $q = 3$ the physics contained in the eigenvalue spectrum displays even more structure. Meyer *et al* [21] investigated this model, using Monte Carlo and analytical methods. They reported a tricritical point in the physical region.

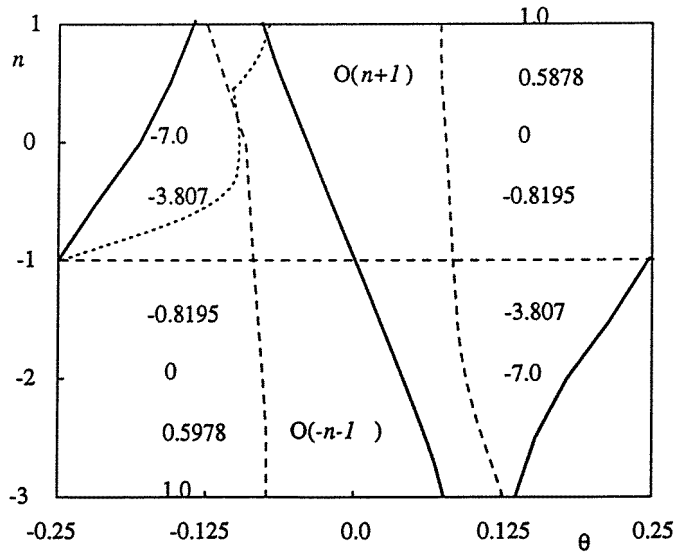

Figure 16. The two regions of different behaviour of branch 0 as a function of n and θ ($s/r = \tan(2\pi\theta)$). The heavy lines represent the first-order transition between the two regions. The physical region of the Potts model is on the right of the dotted line and above the line $n = -1$. The exact solution of branch 0 is indicated by a broken line. For some values of n we have indicated the conformal anomaly c obtained from the transfer matrix calculations at $\theta = -\frac{1}{8}$ and $\theta = \frac{1}{8}$.

For practical reasons the O(n) loop transfer matrix is not suitable to study the behaviour of this Potts model, because the spectrum is dominated by eigenvalues that do not contribute to the partition function. For a study of the Potts model it is more practical to use a transfer matrix using the Potts spin representation. We have done such calculations for the $q = 3$ Potts model along its self-dual line, using helical boundary conditions and finite sizes $L = 2, 3, \ldots, 12$. The self-dual line is characterized by $b = 3$, while a is a free parameter (see equation (32)). Thus we estimated the conformal anomaly, using equation (40), for a range of values of a. The results are shown in figure 17 in terms of a parameter m defined by

$$c = 1 - \frac{6}{m(m+1)}. \tag{42}$$

For not too small values of a the data converge well to $m = 5$ as expected for critical 3-state Potts models [22]. For lower values of a, maxima occur with an apparent convergence to a value close to $m = 6$, as expected for $q = 3$ Potts tricriticality. The extrapolated position of the maximum, i.e. the location of the tricritical point, is $a_{tc} = -0.79(1)$. Thus we confirm the existence of a tricritical point reported by Meyer *et al* [21]. However, the conjectured location [21] $a_{tc} = 0$ is different. In order to obtain further evidence for the tricritical value of a, we have applied transfer-matrix calculations to systems with cylindrical boundary conditions. Evaluation of the two largest eigenvalues yields the magnetic correlation length (equation (39)) from which the magnetic dimension x_m can be estimated (equation (41)). Denoting the estimated dimension $x_L(a)$, one can estimate the tricritical point by solving a numerically from

$$x_L(a) = x_{m,tc} \tag{43}$$

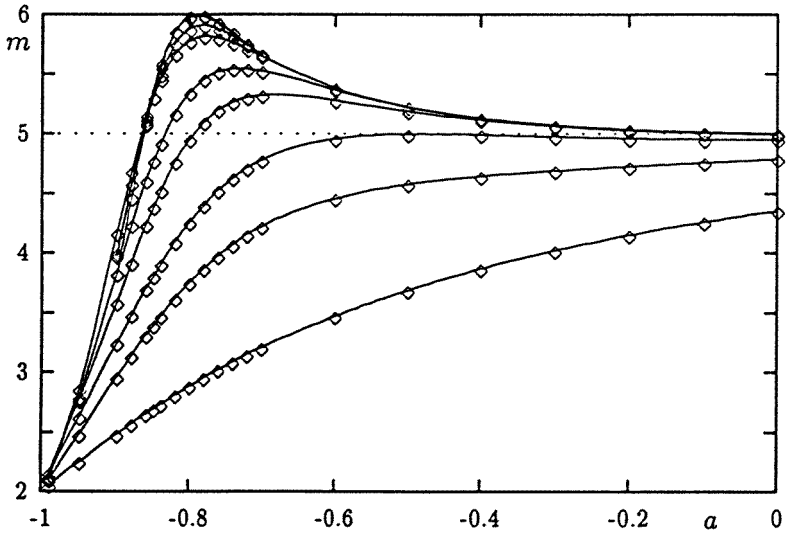

Figure 17. Results for the $q = 3$ Potts conformal anomaly in terms of the parameter m. Data are shown as a function of the nearest-neighbour coupling a for system sizes up to $L = 12$. m_L is calculated from the free energy densities of systems with sizes L and $L - 3$.

where $x_{m,tc} = \frac{2}{21}$ is the tricritical magnetic dimension of the $q = 3$ Potts model. Thus, we obtained a series of estimates of a_{tc} for $L = 2, 3, \ldots, 14$. Extrapolations, whose accuracy was somewhat limited due to alternations for lower L, led to a best estimate $a_{tc} = -0.7856(2)$, in a good agreement with the determination using the maximum of m. As a further consistency check, the largest eigenvalues were calculated at this value of a_{tc} and analysed in order to determine the conformal anomaly. The result $c = 0.857(1)$ or $m = 6.00(2)$ is in a good agreement with $q = 3$ Potts tricriticality.

We return to the dilute loop representation to study branch 1. To obtain the same results for branch 1 as for branch 0, one may add a seam which compensates the minus sign in the weight of loops around the cylinder (see section 4). When this seam is built into the branch-1 transfer matrix, the same results as for branch 0 are obtained. Thus, for branch 1 with a seam there is a region of low-temperature O($n - 1$) behaviour as well as one of low-temperature O($-n + 1$) behaviour.

Next, we determine the conformal anomaly of branch 1. To this purpose we chose periodic boundary conditions, without a seam. The results are summarized in table 4.

These results can also be calculated exactly. Namely, in analogy with equation (31), the O(n) model of branch 1 without a seam is equivalent with the O($-n$) model of branch 0 with a seam. Thus for the dense version of this branch 0 with a seam the contractible loops have a weight $\Delta = -n+1$ and the non-contractible loops have a weight $\Delta' = n+1$. For the corresponding 6-vertex model the conformal anomaly has been calculated both numerically and analytically in [22, 23]. It is given by

$$c = 1 - \frac{6k^2}{h(h-1)} \tag{44}$$

where $\Delta = 2\cos(\pi/h)$ and $\Delta' = 2\cos(k\pi/h)$. Substitution of h and k yields an exact result for the conformal anomaly of branch 1. These results are denoted in the third column of table 4 for values of n between 2 and -1. For these values there is a good agreement between the numerical and the exact data. Notice that the relation between h and k is

Table 4. The numerical and exact result for the conformal anomaly of branch 1. We have used data for finite size 2–6. Estimated uncertainties in the last decimal places are given between parentheses.

n	c_{num}	c_{exact}
2.0	2.70(2)	2.689 294
1.5	1.70(1)	1.696 143
1.0	1.000(5)	1
0.5	0.453(2)	0.452 9104
0.0	0.0000(0)	0
−0.5	−0.37(1)	−0.371 8235
−1.0	−0.6(1)	−0.5

transcendent and that values $c > 1$ are possible. A similar result has already been seen for the tri-tricritical Potts model [7].

8. Conclusions

We have studied the O(n) model on the triangular lattice with the purpose to determine its critical behaviour. New critical behaviour might be expected because on the triangular lattice as much as three loops may collide in a single vertex. Thus we have determined solvable points solving the YB equations for a fully packed loop model on the triangular lattice. However, we only found the solvable points already known from the square lattice.

We have found eight branches of critical points by constructing intersections between the Potts model and O(n) model. We have analysed these branches using transfer-matrix calculations. The critical behaviour of branches 2–5 can be identified by the behaviour of the critical branches on the square lattice. These branches describe O(n) critical behaviour, O(n) low-temperature behaviour, the multicritical behaviour of a model with O(n) and Ising degrees of freedom and the behaviour of a low-temperature O(n) model plus a critical Ising model. The similar behaviour of these branches with critical branches on the square lattice can be understood because each vertex weight on the triangular lattice can be replaced by the weights of three combined Kagomé vertices. The Kagomé weights coincide with the general solution of the critical branches on the square lattice.

The numerical results for branches 6 and 7 do not converge, although the vertex weights can also be replaced by the weights of three combined Kagomé vertices (with the weights of the general solution for the square lattice). We probably find different behaviour to that expected because the boundary conditions for the Kagomé and the square lattice are different.

Branches 0 and 1 contain a free parameter and obey certain symmetry relations. For branch 0 we have observed a first-order transition between a region of low-temperature O($n + 1$) behaviour and a region of low-temperature O($-n - 1$) behaviour. Similar results are observed for branch 1 when a seam is added which compensates a factor of -1 for loops around the cylinder. We have also analysed branch 1 with periodic boundary conditions. We have found exactly and numerically a new result for the conformal anomaly. Values of $c > 2$ occur.

Branch 0 is also equivalent to a q-state Potts model on the triangular lattice, with three-spin coupling in the triangles pointing to the left. q is related to n by $q = (n + 1)^2$. Because the contribution in the partition sum of too many eigenvalues of the transfer matrix

disappear closing the cylinder, it is more practical to study the $q = 3$ Potts model analysing the spin representation of the Potts model. In this way we have located a $q = 3$ tricritical point.

Therefore, our method (construction of intersections) works to find critical points. The behaviour of most of these points are as on the square lattice. The tricritical point of the $q = 3$ Potts model with three-spin coupling in the triangles pointing to the left is new (also found by Meyer *et al* [21]). However, we have not found the multicritical behaviour of ternary collisions of, for example, polymers.

Acknowledgments

We are much indebted to S O Warnaar for valuable discussions. This research is part of the research programme of the FOM ('Stichting voor Fundamenteel Onderzoek der Materie') which is financially supported by the NWO ('Nederlandse Organisatie voor Wetenschappelijk Onderzoek').

References

[1] Nienhuis B 1982 *Phys. Rev. Lett.* **49** 1062
[2] Nienhuis B 1990 *Int. J. Mod. Phys.* B **4** 929
[3] Blöte H W J and Nienhuis B 1989 *J. Phys. A: Math. Gen.* **22** 1415
[4] Domany E, Mukamel D, Nienhuis B and Schwimmer A 1981 *Nucl. Phys.* B **190** 279
[5] Perk J H H and Wu F Y 1986 *Physica* A **138** 100
Perk J H H and Wu F Y 1986 *J. Stat. Phys.* **42** 727
Perk J H H and Schultz C L 1983 Physica **122A** 50
[6] Nienhuis B 1987 *Phase Transitions and Critical Phenomena* vol 11, ed C Domb and J L Lebowitz (London: Academic)
[7] Nienhuis B, Warnaar S O and Blöte H W J 1993 *J. Phys. A: Math. Gen.* **26** 477
[8] Baxter R J 1982 *Exactly Solved Models in Statistical Mechanics* (London: Academic)
[9] Baxter R J, Kelland S B and Wu F Y 1976 *J. Phys. A: Math. Gen.* **9** 397
[10] Warnaar S O, Pearce P A, Seaton K A and Nienhuis B 1994 *J. Stat. Phys.* **74** 469
[11] Izergin A G and Korepin V E 1981 *Commun. Math. Phys.* **79** 303
[12] Batchelor M T, Nienhuis B and Warnaar S O 1989 *Phys. Rev. Lett.* **62** 2425
[13] Batchelor M T and Blöte H W J 1988 *Phys. Rev. Lett.* **61** 138
Batchelor M T and Blöte H W J 1989 *Phys. Rev.* B **39** 2391
[14] Warnaar S O, Batchelor M T and Nienhuis B 1992 *J. Phys. A: Math. Gen.* **25** 3077
[15] Nienhuis B 1990 *Proc. IUPAP Conf. STATPHYS 17 (Rio de Janeiro, 1989)* (Amsterdam: North-Holland)
[16] Enting I G and Wu F Y 1981 *J. Stat. Phys.* **28** 351
[17] Baxter R J, Temperley H N V and Ashley S E 1978 *Proc. R. Soc.* A **358** 535
[18] Pasquier V 1987 *Nucl. Phys.* B **285** 162
Pasquier V 1987 *J. Phys. A: Math. Gen.* **20** L1229
Pasquier V 1987 *J. Phys. A: Math. Gen.* **20** 5707
[19] Blöte H W J and Nightingale M P 1982 *Physica* **112A** 405
[20] Cardy J L 1987 *Phase Transitions and Critical Phenomena* vol 11, ed C Domb and J L Lebowitz (London: Academic)
[21] Meyer H, Anglès d'Auriac J C, Maillard J M, Rollet G and Wu F Y 1995 *Phys. Lett.* A **201** 252
[22] Blöte H W J, Cardy J L and Nightingale M P 1986 *Phys. Rev. Lett.* **56** 742
[23] Hamer C J, Quispel G R W and Batchelor M T 1987 *J. Phys. A: Math. Gen.* **20** 5677